Biophysical Journal, Volume 99

Supporting Material

Experimental evidence for membrane-mediated protein-protein interaction

Ignacio Casuso, Pierre Sens, Felix Rico, and Simon Scheuring

Experimental evidence for membrane-mediated protein-protein interaction

Ignacio Casuso,* Pierre Sens,‡ Felix Rico,* Simon Scheuring *

* Institut Curie, U1006 INSERM, 26 rue d'Ulm, Paris, F-75248 France; and ‡ UMR Gulliver CNRS-ESPCI 7083, 10 rue Vauquelin, Paris, F-75231 France

Address reprint requests and inquiries to Simon Scheuring, Tel.: ++33 (0)1 56 24 67 81; Fax: ++33 (0)1 40 51 06 36; E-mail: simon.scheuring@curie.fr.

SUPPLEMENTAL INFORMATION

SUPPLEMENTAL MATERIAL 1: The ATP synthase of *Halobacterium salinarum*

Nature's use of a transmembrane electrochemical gradient to generate ATP was established in pioneering work by Mitchell (1). According to this, a potential of electrons or protons was used as energy source to phosphorylate ADP. Such a membrane potential can be established by respiration or photosynthesis, the most simple case however is probably the light-induced proton transport of the purple membrane (PM) from *Halobacterium salinarum* densely packed with bacteriorhodopsin (bR) (2). bR activity leads to ATP formation (3) when solely co-reconstituted with ATP-synthases into liposomes (4). bR formed large (~500nm) 2D-arrays (5) sufficiently well ordered to allow determination of the bR structure using electron microscopy (EM) (6). The localization of the proton consuming ATP-synthase and the efficiency of proton migration between bR and ATP-synthase – as it is not inserted into bR arrays – needed to be addressed. It was shown that protons migrate fast and preferentially along the PM surface and reach the edge of bR arrays within ~100μs (7). This mechanism allows the ATP-synthases to be located at the edges of the bR 2D-arrays, but there is no experimental evidence so far concerning its location, association and dynamics.

Little is known about the ATP-synthase of the extremely halophilic archaebacterium *Halobacterium salinarum*. Sequence analysis have shown that this A-ATP-synthase (A for archaebacterial) is related to the F-ATP-synthase and to the eukaryotic V-ATPase (8, 9). A low-resolution single particle EM 3D-map of an A-ATP-synthase (10) showed that the overall shape resembled the F-ATP-synthase (11), though two peripheral stalks were found (10). Many aspects of the structure of the F-ATP-synthase were solved (12, 13). The c-ring structures of bacterial Na^+- (14) H^+- (15) ATP-synthases are solved, as well as the chloroplast H^+- ATP-synthase (16) and a V-type Na^+- ATPase (17). ATP-synthases form dimers in mitochondria (18-20), but they are thought to occur as monomers in prokaryotes, and no information is available, to our knowledge, on this topic about the A-ATP-synthase.

SUPPLEMENTAL MATERIAL 2: High-speed atomic force microscope (HS-AFM) observation of purple membranes

Purple membranes (PM) from *Halobacterium salinarum* containing wild type bacteriorhodopsin (bR) were isolated according to Oesterhelt and Stoeckenius (2). PM patches were deposited on freshly cleaved mica. To check the cleavage quality the mica was first imaged in adsorption buffer containing 10 mM Tris–HCl (pH 7.6), 150 mM KCl, 25 mM MgCl2. Subsequently 3 μl of PM solution was injected into the adsorption buffer drop on the mica surface. After 15 minutes the sample was rinsed with ten volumes recording buffer containing 10 mM Tris–HCl (pH 7.6), 150 mM KCl.

AFM (21) has proven a powerful tool for membrane protein research. It allowed watching the native supramolecular membrane protein assembly of prokaryotes (22-24) and eukaryotes (25, 26). Early it has been used to study PM (27). Despite attempts to assess membrane dynamics using conventional AFM setups (28-30), the dawn of HS-AFM (31) had to be awaited for monitoring dynamic processes (32, 33). HS-AFM (31) has evolved through a series of improvements (34, 35), and allows now imaging at up to 50 ms frame acquisition speed. If only a few scan lines are recorded topographic acquisition is faster than 1 ms. At this high imaging frequency molecular motor action (36), enzymatic activity (37), and 2D-diffusion dynamics (32, 33, 38), could be studied.

The observations of PMs by HS-AFM (31) were performed in oscillating mode using an amplitude reduction ratio of 30%. A high-sensitivity photodetector has been implemented and the photodetector signal was low-pass filtered (pass ≤ 5 MHz). Cantilevers designed for high-speed AFM from (Olympus, Tokyo, Japan) with about 8 μm length and a spring constant of 0.1–0.2 N/m, a resonance frequency of 0.8–1.2 MHz and a quality factor of ~2 in solution were

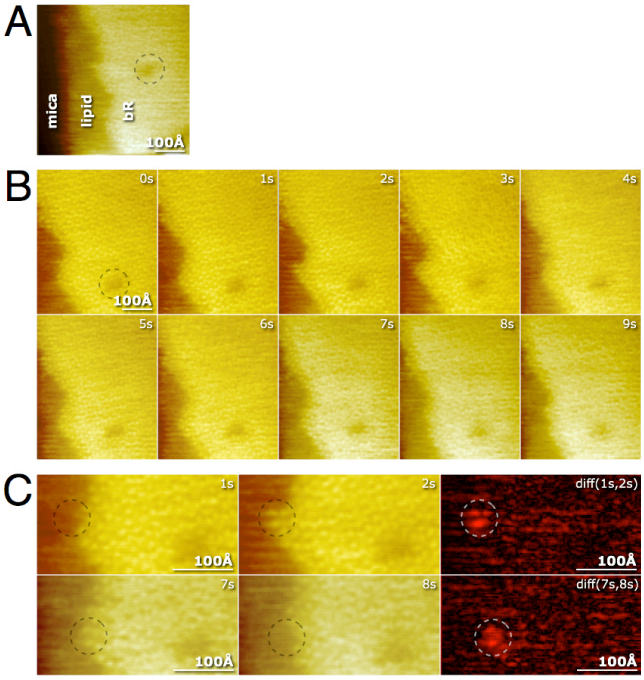

Fig. S1) Dynamics of bR in lipid border regions of purple membranes of *Halobacterium salinarum*. A) Overview topograph. Three image regions can be depicted, the mica support, the lipid bilayer and the bR lattice within the bilayer. **B)** Ten images from a longer sequence: The shape of the bR-lattice edge changes with time. The membrane depression (dashed outline in frame 0s) allowed image alignment with the overview image A). **C)** Detailed analysis (left: image at time t, middle: image at time t+1s, right: difference image (t,t+1s)) of the association (top) and the dissociation of individual bR trimers to and from the bR-array (full false color scale: 29Å).

used (39) featuring an electron beam deposition (EBD) tip at the end of the microfabricated pyramidal tip (40). The sensitivity of the AFM system to the probe deflection was of 0.1 V/nm. The scan areas were of 500 x 500 $(Å)^2$, and the number of pixels per frame was of 100×100. The imaging rates were 1000ms (Movie S1) and 187ms (Movie S2) per frame.

SUPPLEMENTAL MATERIAL 3: Topography and mass spectrometry assignment of *Halobacterium salinarum* ATP synthase c-ring

In the edge-region of PM, we found ring-shaped molecules with 65-Å diameter (**Fig. S2A**). Based on their shape, size and location besides the bR-arrays we attributed the protein to membrane standing ATP-synthase c-rings. This attribution was confirmed by mass-spectrometry analysis that documented the presence of two peptides with masses of 7517 Da and 7618 Da. The entire c-ring subunit gene (*atpk*) of *H. salinarum* codes for a 89 amino acids long hydrophobic protein (CAP14578, (41)). However it has been shown that the N-terminal 12 amino acids of the c-ring subunits in the membrane were cleaved (42). The calculated mass of the remaining membranous protein is 7516.84 Da in extremely good agreement with the 7517 Da measured (**Fig. S2B**). The finding of a second peak at 7618 Da is evidence for alternative protein cleavage resulting in a one amino acid longer protein.

SUPPLEMENTAL MATERIAL 4: Sequence alignment with other c-ring proteins

In order to get more insight into the A-type ATP-synthase subunit K (*atpk*; CAP14578; (41)) structure, we have perfomed sequence alignment with the c-ring proteins of known structure: chloroplast H^+-ATP-synthase (16), bacterial Na^+- ATP-synthase from *I. tartaricus* (14) and the bacterial H^+- ATP-synthases (15) from *S. platensis* (**Fig. S3A**). The *H. salinarum* subunit K compares with these proteins in light of the fact that they consist of two transmembrane helices. It has been reported that sequence-wise the A-type ATP synthase compared slightly better with V-type ATPases (8), though their c-ring is constituted of multiplications of the two-helix unit. Therefore, we have also performed sequence comparison with the first and second halfes of the c-ring subunit of the V-type ATPase from *E. hirae* (**Fig. S3B**) of which the structure is known (17). All information points to the presence of two transmembrane helices in the c-ring structure of *H. salinarum* that span approximately from M19 to A55 and from L59 to P86. Of particular interest for our work is the second transmembrane helix, because it is the lipid membrane exposed: we estimate that the charged D58 can not yet be membrane embedded and that P86 breaks the transmembrane helix where the chloroplast, the *I. tartaricus*, and the *S. platensis* c-ring structures terminate their helices with a conserved Leucine. The membrane exposed transmembrane helix can therefore be estimated of approximately 28 amino acids and 42 Å in length. In all structures the helices are fairly perpendicular with respect to the membrane plane. Sequences analysis for transmembrane domain prediction using TMpred (http://www.ch.embnet.org/software/TMPRED_form.html) provided a similar picture (**Fig. S3C**).

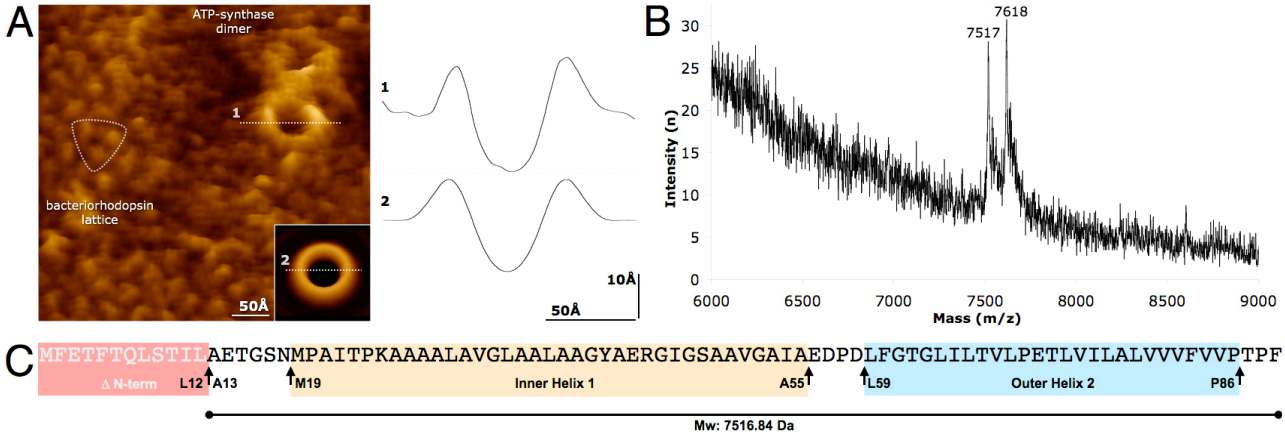

Fig. S2) Assignment of ATP-synthase c-ring structures in purple membranes of *H. salinarum*. A) AFM image of the cytoplasmic face of purple membrane containing bR-trimers (triangular outline) besides c-rings (full false color scale: 18Å, inset: radial symmetrized c-ring average (*n*=106)). Section profiles of raw data (1) and averaged (2) c-rings. The ring diameter is 65Å ± 5Å (*n*=106). **B)** Mass spectrometry analysis of PM. Besides a major peak corresponding to bacteriorhodopsin at ~28kDa, two peaks at 7517 Da and 7618 Da were found. **C)** *H. salinarum* subunit K (c-ring) sequence. The first 12 N-terminal amino acids are cleaved (red box) (8). Based on sequence alignment with c-ring proteins of known structure (Supplemental Material 3) the positions of the inner (orange box) and outer (blue box) transmembrane helices are proposed.

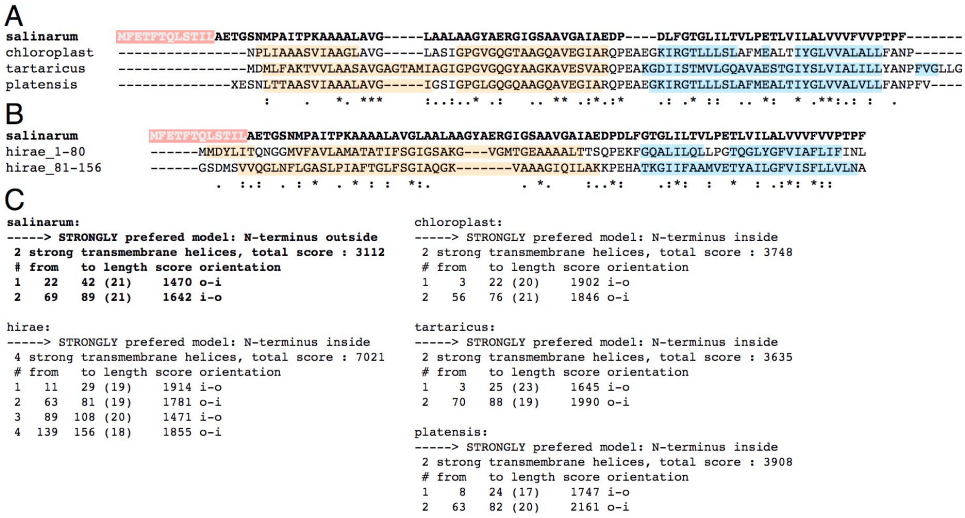

Fig. S3) Sequence analysis of *H. salinarum* A-type ATP-synthase c-ring subunit K (*atpk*; CAP14578). A) Sequence comparison with the chloroplast, the *I. tartaricus*, and the *S. platensis* c-ring sequences, c-rings of which the structure has been solved (2W5J, 2WGM, 2WIE). **B)** Sequence comparison with the E. hirae V-ATPase c-ring sequence (2BL2). The transmembrane helix regions in the structures (2W5J, 2WGM, 2WIE, 2BL2) are shaded in A) and B). The first 12 aminoacids in the H. salinarum sequence are cleaved in the membrane (8). **C)** C-ring sequences analyses for transmembrane regions by TMpred (http://www.ch.embnet.org/software/TMPRED_form.html).

SUPPLEMENTAL MATERIAL 5: Analysis of molecular motion

To define the molecular positions of the c-rings in the AFM images, for all analyses presented in this work, we used a "doughnut"-shaped reference, i.e. a radial symmetrized c-ring average (**Fig. S2A**, inset), that was cross-correlated with the topographs. Cross correlation of a perfectly ring-shaped motif with a approximately ring-shaped molecule unambiguously and precisely defines the molecular center position. Supplementary figure S4 shows particle-tracking diagrams of a HS-AFM movie of sixty frames recorded at a frame rate of 187 ms, where the c-rings were imaged as *close dimer*, *elongated dimer* and *monomer*. The real space positions of the c-rings (**Fig. S4A**) were treated concerning their Y- (**Fig. S4B**) and X- (**Fig. S4C**) coordinates. From this, the angular assembly of the dimer was deduced that remained well conserved over time, even after c-ring dissociation and re-association (**Fig. S4D, top**).

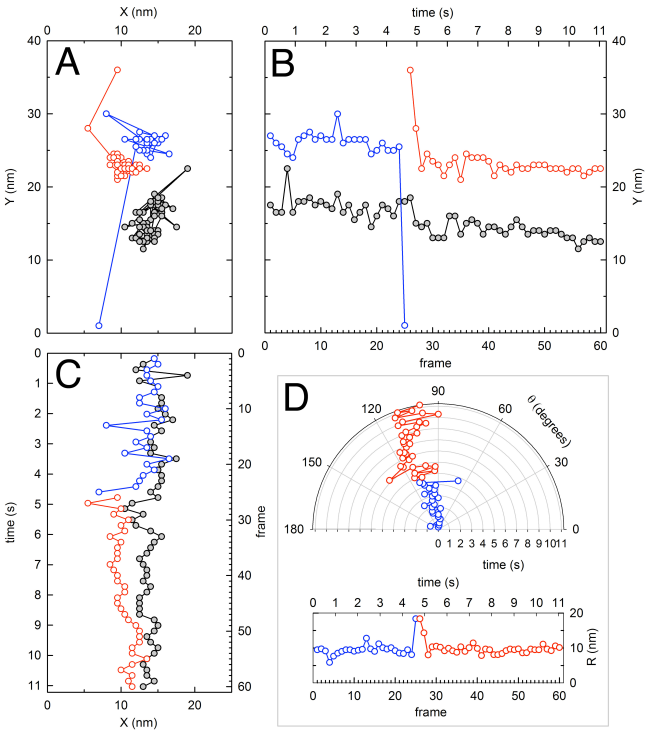

Fig. S4) ATP-synthase c-rings tracking. Black dots and lines denote the c-ring remaining in the imaging frame during entire HS-AFM analysis (see figure 1 in the main manuscript and supplementary movie 2), red and blue dots and lines represent trajectories of alternating c-rings. A) Real-space representation of particle tracking. B) and C) projections onto the Y- and X- coordinates respectively, as a function of time. D) Polar coordinates and center-to-center distance representation of the c-ring diffusion.

We suspect that the angular assembly preservation is facilitated by remaining stator elements (Supplemental Material 6). Most often inter-ring distances of 10 nm were found (frames 1-23 and frames 29-60) (**Fig. S4D, bottom**), with a period during which dimer dissociation occurred (frames 24-28); the monomer c-ring detection is limited by the imaging frame size and acquisition rate.

The motion of molecules was analyzed by computing the mean square displacement (MSD) following

$$MSD(\Delta t) = \left\langle \left[r_{(t+\Delta t)} - r_{(t)} \right]^2 \right\rangle$$

where r is the position of each molecule, Δt is the lag-time and the $\langle brackets \rangle$ indicate that the average was calculated over the elapsed time t. The results were fitted with a generalization of the diffusion equation ($MSD = 4D\Delta t$) for complex systems:

$$MSD = \Gamma \cdot \Delta t^{\alpha}$$

where Γ is a scale factor independent of time, and α is the anomalous diffusion exponent. If the exponent $\alpha > 1$ motion is called to be super-diffusive, if $\alpha = 1$ is free diffusive, and if $\alpha < 1$ is called sub-diffusive.

SUPPLEMENTAL MATERIAL 6: Stator elements of the ATP synthase

The angular association preservation (see figure S4D top) of the c-rings within the dimer implies an additional element on the c-ring surface that defines the orientation within the membrane plane. This is particularly obvious when the dimer temporarily dissociated and reformed with similar angular arrangement. Indeed, additional peripheral protein structure, attributed to the transmembrane part of the ATP-synthase stator, was imaged at preserved localization besides the dimer (**Fig. S5A, B**) and the monomer (**Fig. S5C**). Doubtlessly the stator defines the rotational orientation of the ATP-synthase within the membrane plane and confines therefore where the partner ATP-synthase within the dimer can dock to the assembly.

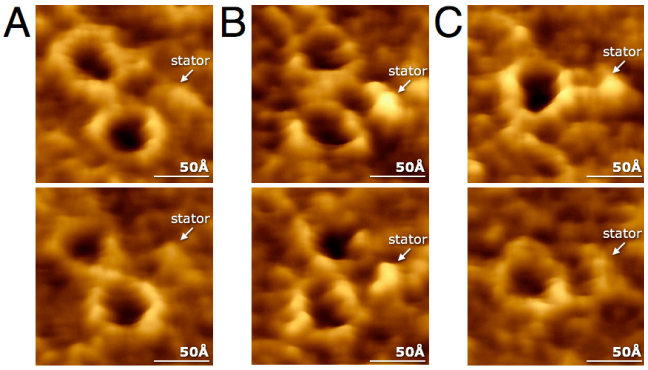

Fig. S5) ATP-synthase stator defines angular assembly preservation (full false color scale: 18Å). Two images of longer sequences are shown of ATP-synthase dimers in **A)** and **B)** and of a ATP-synthase monomer in **C)**, in which a peripheral protein protrusion is visible. The location of this remains constant and is attributed to the transmembrane stator. The localization of the stator confines the angular assembly of the dimer.

SUPPLEMENTAL MATERIAL 7: Topography of the lipids surrounding the two interacting C-ring proteins

The hydrophobic thickness of the c-rings is about 10Å larger than the hydrophobic thickness of the lipid bilayer. In these conditions the hydrophobic mismatch theory predicts significant increase of the lipid bilayer thickness in the region between the two c-rings. Our AFM data partially corroborates this hypothesis, it has been found that 55% of the frames where the c-rings were found in an elongated dimer assembly presented an increased lipid bilayer thickness in the region between the two c-rings. These results should be interpreted conservatively as possible sources of error such as the tip convolution and the acquisition noise may play a role.

Two different types of features have been observed in the frames where the lipid thickness between the c-rings was increased. On the one hand, an elevated (~ 10Å) flat plateau **(Fig. S6A, B)**, this has been only observed for inter c-

ring center-to-center distances from 105 to 120Å. On the other hand an elevated plateau with a central protrusion peak around 10Å high that spans from c-ring to c-ring **(Fig. S6C, D)**. This second feature is only observed for inter c-ring distances below 100Å. We interprete the latter effect is due to tip convolution, i.e. the tip can not enter between the two narrow located rings. This however makes us confident that the flat plateau that we can observe between elongated c-rings are indeed elevated lipid molecules accomodating for the c-ring hydrophobic mismatch.

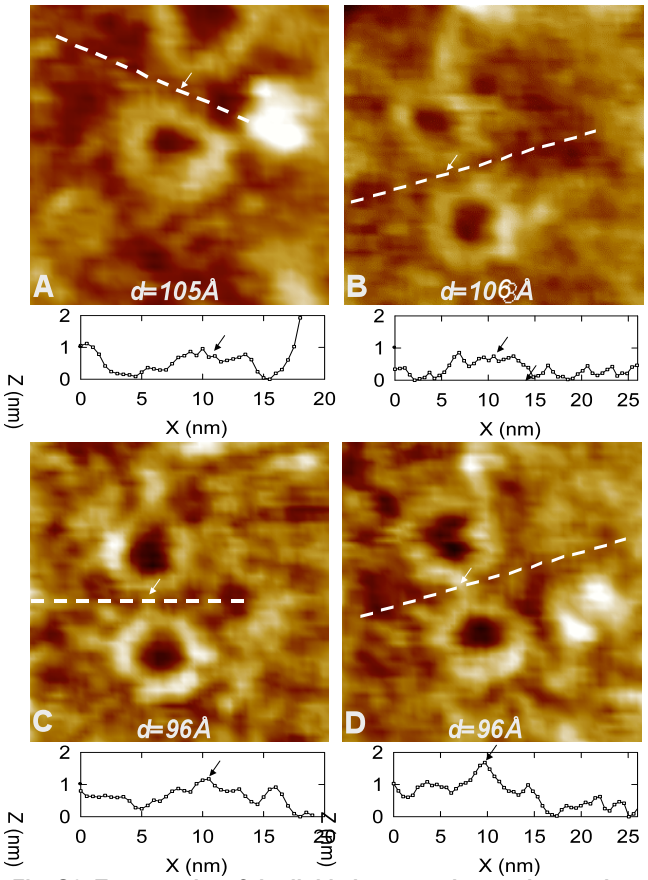

Fig. S6. Topography of the lipids between the two interacting C-ring proteins. ***(d)*** **indicates the c-ring center-to-center distance** (full false color scale: 18Å). The images **A)** (d= 105Å) **B)** (d= 106Å) show the presence of an elevated flat plateau profiles between the C-rings. The images **C)** (d= 96Å) and **D)** (d= 96Å) with shorter distances between the C-rings present additional protrusions spanning between the C-rings (arrows).

SUPPLEMENTAL MATERIAL 8: Theoretical considerations

Hydrophobic mismatch between a membrane inclusion and the surrounding lipid bilayer creates a deformation of the bilayer that extends a small distance λ around the inclusion (43). It can be shown (43) that it is set by the ratio of the membrane bending rigidity κ and stiffness to stretching k, according to $\lambda = (\kappa\, h^2 / k)^{1/4}$. One expects from scaling arguments that both elastic constants are related to the bilayer Young's modulus (E) according to $\kappa \sim E\, h^3$ and $k \sim E\, h$, (where h is the bilayer thickness) predicting a decay length of order the bilayer thickness.

If two such inclusions are sufficiently close for their associated membrane deformation fields to overlap, they experience a membrane-mediated interaction, which is generally attractive between similar inclusions. Although numerous theoretical and numerical studies have explored various aspects of membrane-mediated interactions between membrane proteins (for a review, see (43)), direct experimental evidence for such interaction have not been obtained until now. The strength of the interaction potential depends on the elastic properties of the membrane (such as its bending energy κ, and the membrane decay length λ) and the hydrophobic thickness mismatch Δh. The precise expression of the potential can be difficult to calculate (see for instance (44)) but it typically decays exponentially over the characteristic length λ. Between to disc-like inclusions whose radius R is much larger than λ, it can be approximated by the integral over the discs curved boundaries of the energy density of membrane deformation between two flat walls:

$$U_{membrane}(d) = 2\kappa\left(\frac{\Delta h}{\lambda}\right)^2\sqrt{\pi\frac{R}{\lambda}}e^{-(d-2R)/\lambda}$$

where d is the distance between the centers of the two discs. When the proteins are in contact, attraction still occurs, but bringing the rings closer to one another requires deforming them (rearranging the membrane exposed amino acid side chains or deforming the strongly bound lipid layer surrounding them). This involves an elastic cost which can be estimated by analogy with the Hertz contact problem (45):

$$U_{elastic}(d) = \frac{\pi}{16}k(d-2R)^2$$

where k is the elastic modulus of the deformed body. Assuming that the data (see figure 2A in the main manuscript) represent an accurate measure of the equilibrium probability distribution for the distance between the two rings: $p(d) = p_\infty e^{-(U_{membr}(d)-U_{elast}(d))/kT}$, one can fit the experimentally measured interaction potential and estimate the different physical parameters (see figure 2B in the main manuscript). The data was best fitted using the following parameters: 2R=103Å, λ = 20 Å, k = 0.06 k_BT / Å^2 and $e_0 = \kappa\,\Delta h^2/\lambda^2 = 0.8\ k_B$T .

We find that the elastic modulus is $k = 0.025$J/m^2 is an order of magnitude lower than the elastic modulus of lipid bilayers (0.2 J/m^2). The decay length λ is indeed of order the bilayer thickness, and taking a hydrophobic monolayer mismatch Δh = 5 Å, (lipid bilayer thickness of about 30Å (46, 47), protein hydrophobic thickness of about 40Å), a good fit for the bending modulus is κ = 13 k_BT, which is also in agreement with expected values.

SUPPLEMENTAL MOVIE 1 title:
Dynamics of bR in lipid border regions of purple membranes of *Halobacterium salinarum*

SUPPLEMENTAL MOVIE 2 title:
ATP-synthase c-ring motion monitored by high-speed atomic force microscopy (HS-AFM)

REFERENCES AND FOOTNOTES

1. Mitchell, P. 1961. Coupling of Phosphorylation to Electron and Hydrogen Transfer by a Chemi-Osmotic type of Mechanism. Nature 191:144-148.
2. Oesterhelt, D., and W. Stoeckenius. 1973. Functions of a new photoreceptor membrane. Proc Nat Amer Soc 70:2853-2857.
3. Racker, E., and W. Stoeckenius. 1974. Reconstitution of purple membrane vesicles catalyzing light-driven proton uptake and adenosine triphosphate formation. J Biol Chem 249:662-663.
4. Yoshida, M., N. Sone, H. Hirata, and Y. Kagawa. 1975. ATP synthesis catalyzed by purified DCCD-sensitive ATPase incorporated into reconstituted purple membrane vesicles. Biochem Biophys Res Commun 67:1295-1300.
5. Henderson, R., and P. N. T. Unwin. 1975. Three-dimensional model of purple membrane obtained by electron microscopy. Nature 257:28-32.
6. Henderson, R., J. M. Baldwin, T. A. Ceska, F. Zemlin, E. Beckman, and K. H. Downing. 1990. Model for the structure of bacteriorhodopsin based on high-resolution electron cryo-microscopy. J. Mol. Biol. 213:899-929.
7. Heberle, J., J. Riesle, G. Thiedemann, D. Oesterhelt, and N. A. Dencher. 1994. Proton migration along the membrane surface and retarded surface to bulk transfer. Nature 370:379-382.
8. Ihara, K., T. Abe, K. I. Sugimura, and Y. Mukohata. 1992. Halobacterial A-ATP synthase in relation to V-ATPase. J Exp Biol 172:475-485.
9. Nanba, T., and Y. Mukohata. 1987. A membrane-bound ATPase from Halobacterium halobium: purification and characterization. J Biochem 102:591-598.
10. Vonck, J., K. Pisa, N. Morgner, B. Brutschy, and V. Müller. 2009. Three-dimensional structure of A1A0 ATP synthase from the hyperthermophilic archaeon Pyrococcus furiosus by electron microscopy. J Biol Chem. 284:10110-10119.
11. Rubinstein, J. L., J. E. Walker, and R. Henderson. 2003. Structure of the mitochondrial ATP synthase by electron cryomicroscopy. EMBO J 22:6182-6192.
12. Abrahams, J. P., A. G. W. Leslie, R. Lutter, and J. E. Walker. 1994. Structure at 2.8 angstrom resolution of F_1-ATPase from bovine heart mitochondria. Nature 370:621-628.
13. Stock, D., A. G. Leslie, and J. E. Walker. 1999. Molecular architecture of the rotary motor in ATP synthase. Science 286:1700-1705.
14. Meier, T., P. Polzer, K. Diederichs, W. Welte, and P. Dimroth. 2005. Structure of the rotor ring of F-Type Na+-ATPase from Ilyobacter tartaricus. Science 308:659-662.
15. Pogoryelov, D., O. Yildiz, J. D. Faraldo-Gomez, and T. Meier. 2009. High-resolution structure of the rotor ring of a proton-dependent ATP synthase. Nat Struct Mol Biol 16:1068-1073.
16. Vollmar, M., D. Schlieper, M. Winn, C. Büchner, and G. Groth. 2009. Structure of the c14 rotor ring of the proton translocating chloroplast ATP synthase. J Biol Chem 284:18228-18235.
17. Murata, T., I. Yamato, Y. Kakinuma, A. G. W. Leslie, and J. E. Walker. 2005. Structure of the rotor of the V-type Na+-ATPase from Enterococcus hirae Science 308:654-659.
18. Paumard, P., J. Vaillier, B. Coulary, J. Schaeffer, V. Soubannier, D. M. Mueller, D. Brèthes, J.-P. di Rago, and J. Velours. 2002. The ATP synthase is involved in generating mitochondrial cristae morphology. EMBO J 21:221-230.
19. Buzhynskyy, N., P. Sens, V. Prima, J. N. Sturgis, and S. Scheuring. 2007. Rows of ATP synthase dimers in native mitochondrial inner membranes. Biophys J 93:2870-2876.
20. Strauss, M., G. Hofhaus, R. R. Schroeder, and W. Kuhlbrandt. 2008. Dimer ribbons of ATP synthase shape the inner mitochondrial membrane EMBO J 27:1154-1160.
21. Binnig, G., C. F. Quate, and C. Gerber. 1986. Atomic force microscope. Phys. Rev. Lett. 56:930-933.
22. Bahatyrova, S., R. N. Frese, C. A. Siebert, J. D. Olsen, K. O. Van Der Werf, R. van Grondelle, R. A. Niederman, P. A. Bullough, and C. N. Hunter. 2004. The native architecture of a photosynthetic membrane. Nature 430:1058-1062.
23. Scheuring, S., J. Seguin, S. Marco, D. Levy, B. Robert, and J. L. Rigaud. 2003. Nanodissection and high-resolution imaging of the Rhodopseudomonas viridis photosynthetic core complex in native membranes by AFM. Proc Nat Amer Soc USA 100:1690-1693.
24. Scheuring, S., and J. N. Sturgis. 2005. Chromatic adaptation of photosynthetic membranes. Science 309:484-487.
25. Buzhynskyy, N., R. K. Hite, T. Walz, and S. Scheuring. 2007. The supramolecular architecture of junctional microdomains in native lens membranes. EMBO Reports 8:51-55.
26. Fotiadis, D., Y. Liang, S. Filipek, D. A. Saperstein, A. Engel, and K. Palczewski. 2003. Atomic-force microscopy: Rhodopsin dimers in native disc membranes. Nature 421:127-128.
27. Müller, D. J., F. A. Schabert, G. Büldt, and A. Engel. 1995. Imaging purple membranes in aqueous solutions at subnanometer resolution by atomic force microscopy. Biophys. J. 68:1681-1686.
28. Müller, D. J., A. Engel, U. Matthey, T. Meier, P. Dimroth, and K. Suda. 2003. Observing membrane protein diffusion at subnanometer resolution. J. Mol. Biol. 327:925-930.
29. Scheuring, S., N. Buzhynskyy, S. Jaroslawski, R. P. Goncalves, R. K. Hite, and T. Walz. 2007. Structural models of the supramolecular organization of AQP0 and connexons in junctional microdomains. J Struct Biol 160:385-394.

30. Scheuring, S., and J. N. Sturgis. 2006. Dynamics and diffusion in photosynthetic membranes from Rhodospirillum Photometricum. Biophysical Journal 91:3707-3717.
31. Ando, T., N. Kodera, E. Takai, D. Maruyama, K. Saito, and A. Toda. 2001. A high-speed atomic force microscope for studying biological macromolecules. Proc Nat Amer Soc 98:12468-12472.
32. Casuso, I., N. Kodera, C. Le Grimellec, T. Ando, and S. Scheuring. 2009. Contact-mode high-resolution high-speed atomic force microscopy movies of the purple membrane. Biophys J 97:1354-1361.
33. Yamashita, H., K. Voitchovsky, T. Uchihashi, C. S.A., J. F. Ryan, and T. Ando. 2009. Dynamics of bacteriorhodopsin 2D crystal observed by high-speed atomic force microscopy. J Struct Biol 167:153-158.
34. Kodera, N., H. Yamashita, and T. Ando. 2005. Active damping of the scanner for high-speed atomic force microscopy. Review of Scientific Instruments 76.
35. Kodera, N., M. Sakashita, and T. Ando. 2006. Dynamic proportional-integral-differential controller for high-speed atomic force microscopy. Review of Scientific Instruments 77:083704-083707.
36. Kodera, N., T. Kinoshita, T. Ito, and T. Ando. 2003. High-resolution imaging of myosin motor in action by a high-speed atomic force microscope. Adv Exp Med Biol 538:119-127.
37. Yokokawa, M., C. Wada, T. Ando, N. Sakai, A. Yagi, S. H. Yoshimura, and K. Takeyasu. 2006. Fast-scanning atomic force microscopy reveals the ATP/ADP-dependent conformational changes of GroEL. Embo J 25:4567-4576.
38. Yamamoto, D., T. Uchihashi, N. Kodera, and T. Ando. 2008. Anisotropic diffusion of point defects in two-dimensional crystal of streptavidin observed by high-speed atomic force microscopy. Nanotechnol:doi: 10.1088/0957-4484/1019/1038/384009.
39. Kitazawa, M., K. Shiotani, and A. Toda. 2003. Batch fabrication of sharpened silicon nitride tips. Japanese Journal of Applied Physics Part 1-Regular Papers Short Notes & Review Papers 42:4844-4847.
40. Ando, T., T. Uchihashi, N. Kodera, A. Miyagi, R. Nakakita, H. Yamashita, and M. Sakashita. 2006. High-speed atomic force microscopy for studying the dynamic behavior of protein molecules at work. Japanese Journal of Applied Physics Part 1-Regular Papers Brief Communications & Review Papers 45:1897-1903.
41. Pfeiffer, F., S. C. Schuster, A. Broicher, M. Falb, P. Palm, K. Rodewald, A. Ruepp, J. Soppa, J. Tittor, and D. Oesterhelt. 2008. Evolution in the laboratory: the genome of Halobacterium salinarum strain R1 compared to that of strain NRC-1. Genomics 91:335-346.
42. Ihara, K., S. Watanabe, K. I. Sugimura, I. Katagiri, and Y. Mukohata. 1997. Identification of proteolipid from an extremely halophilic archeon Halobacterium salinarum as an N,N'-Dicyclohexyl-carboiimide binding subunit of ATP synthase. Archives of Biochemistry and Biophysics 341:267-272.
43. Phillips, R., T. Ursell, P. Wiggins, and P. Sens. 2009. Emerging roles for lipids in shaping membrane-protein function. Nature 459:379-385.
44. Dan, N., P. Pincus, and S. A. Safran. 1993. Membrane-induced interactions between inclusions. Langmuir 9:2768-2771.
45. Johnson, K. L. 1985. Contact Mechanics. Cambridge University Press, Cambridge, UK.
46. Renner, C., B. Kessler, and D. Oesterhelt. 2005. Lipid composition of integral purple membrane by 1H and 31P NMR. J Lipid Res 46:1755-1764.
47. Dumas, F., M. C. Lebrun, and J. F. Tocanne. 1999. Is the protein/lipid hydrophobic matching principle relevant to membrane organization and functions? Febs Lett 458:271-277.